Mapping and interpretation of satellite magnetic anomalies from POGO data over the Antarctic region

Michael E. Purucker ([1]), **Ralph R.B. von Frese** ([2]) **and Patrick T. Taylor** ([3])
([1]) *Raytheon ITSS at Geodynamics Branch, Goddard Space Flight Center, Greenbelt, MD, U.S.A.*
([2]) *Byrd Polar Research Center and Department of Geological Sciences, The Ohio State University, Ohio, U.S.A.*
([3]) *NASA, Geodynamics Branch, Goddard Space Flight Center, Greenbelt, MD, U.S.A.*

Abstract
A satellite magnetic anomaly map made using the POGO magnetic field data is compared to three maps made using Magsat data. A total of 14 anomalies with magnitudes greater than 3 nT can be identified in all four of the maps poleward of 60°S latitude. Forward models of the Antarctic continental and oceanic lithosphere are produced which use magnetic crustal thickness based on seismic and heat flow data, and which also use the distribution of the Cretaceous Quiet Zone from marine geophysics. These simple models can explain significant parts of eight of the 14 identified anomalies. The remaining anomalies may be caused by lateral variations of magnetization, inadequate models of the magnetic crustal thickness, or remanent magnetizations in directions other than the present field. In addition, contamination of the magnetic anomaly maps by fields of time-varying external origin (and their corresponding internal parts) is still a significant problem in the Antarctic region.

Key words *Antarctic – geomagnetic field – magnetic field satellites – magnetic anomalies*

1. Introduction

The POGO (Polar Orbiting Geophysical Observatories) satellites (Cain *et al.*, 1967) were the first satellites to map the Earth's magnetic field with the accuracy necessary to resolve features of lithospheric origin (Regan *et al.*, 1975). Flying between 1967 and 1971, the POGOs were followed by Magsat (Magnetic field satellite) in 1979. Magsat improved upon the POGOs by including vector magnetometers in addition to the scalar magnetometers included on the POGOs. While the error estimates from all known sources were comparable between POGO and Magsat, the vector magnetometers on Magsat allowed for a better separation among the multiple magnetic field sources encountered in the near-Earth environment (Langel, 1982).

The signal to noise ratio for crustal anomalies at satellite altitude over the polar regions is no better than 4 to 1 (Arkani-Hamed *et al.*, 1994) whereas at aircraft altitude the signal to noise ratio is more commonly 100 to 1 or better. This limitation of the satellite anomaly data drives the development of models that can simultaneously separate the multitude of magnetic fields encountered by the satellite (Langel *et al.*, 1996), in contrast to the sequential approach used in aeromagnetic data reduction.

External field variability is largest near the magnetic poles, both north and south. This variability can be seen in the map of the standard error of the POGO data (fig. 1). The standard

Mailing address: Dr. Michael Purucker, Geodynamics Branch, Goddard Space Flight Center, Greenbelt, MD 20771, U.S.A.; e-mail: purucker@geomag.gsfc.nasa.gov

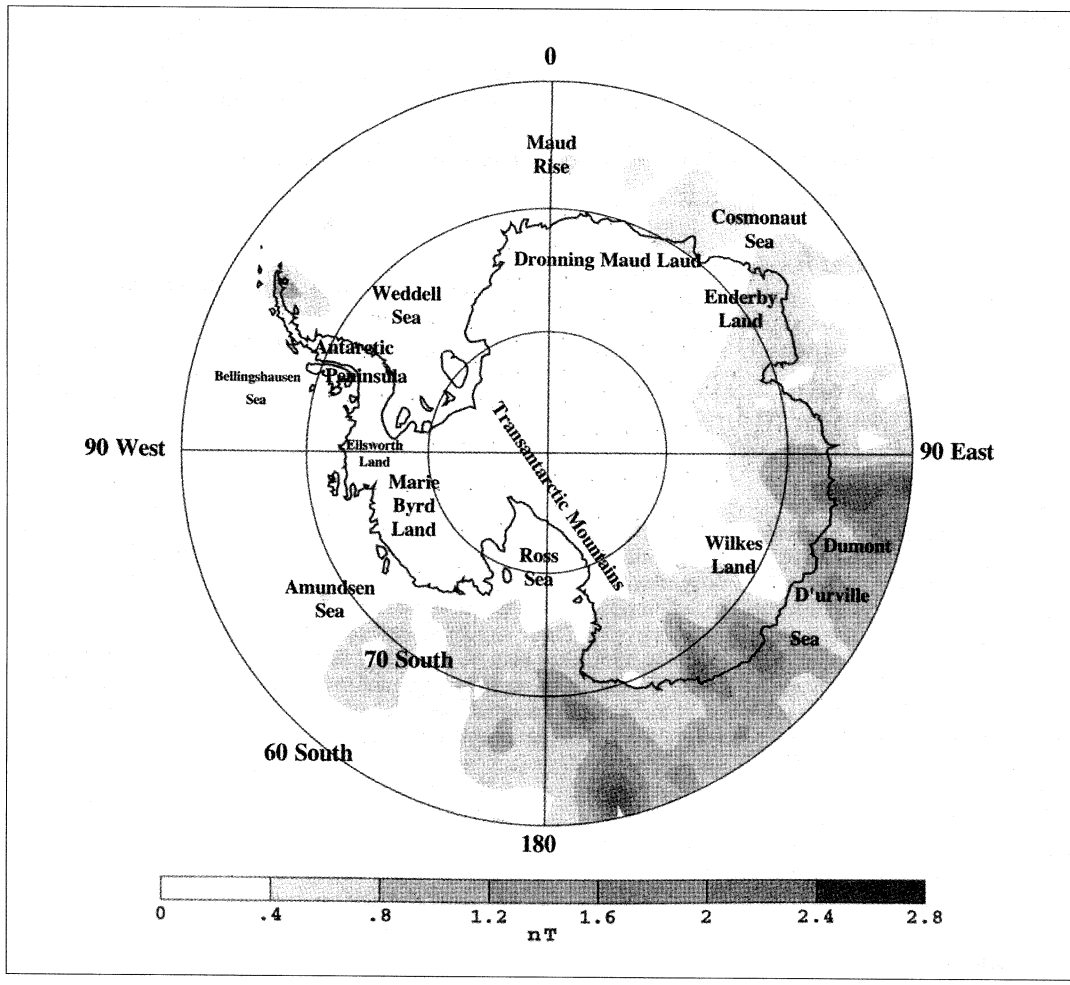

Fig. 1. The standard error of the average POGO scalar anomaly map of Langel (1990). Locations discussed in the text are also included on the map. Stereographic projection. Average altitude of the data is 500 km. Units are nT.

error of the mean is defined as $\frac{\sigma}{\sqrt{N}}$ where σ is the standard deviation of the N data points in each 3° by 3° bin. The variability can be seen to be largest in an arc enveloping the South Magnetic Pole (67°S, 140°E). The polar and near-polar current systems, at altitudes of 100-400 km, are significantly more complicated than those at mid- and low-latitudes because of the greater influence of the magnetic field of the solar wind at high latitudes.

The variability of the external magnetic field can be turned to advantage in constructing anomaly maps over the Antarctic. Because the anomaly field is static, extraction of common features in maps made at different local times, seasons, or by different satellites should yield a map of static magnetic field originating from the lithosphere. That is the essence of the approach pursued in this paper, and has been central to all other attempts to construct anomaly maps in the

Antarctic (Cain *et al.*, 1990; Langel, 1990; Alsdorf *et al.*, 1994; Arkani-Hamed *et al.*, 1994). There are some caveats to this approach. Obviously, a current system that is unchanged between dawn and dusk will mimic a magnetic anomaly in the Magsat data. Our state of ignorance is such that we can not say with certainty that there are no such current systems. POGO, on the other hand, flew at all local times and so should have fewer problems with regards to overhead current systems. Of more importance is the internal response to time-varying external current systems. A time-varying external field will induce an internal magnetic field. Because the electrical conductivity of the oceans that surround the Antarctic is considerably greater than that of the Antarctic continental crust, the magnetic field induced in the oceans (by, for example, the daily solar quiet (S_q) variation) can be very similar at local dawn and dusk (Tarits *et al.*, 1997; Olsen, 1999).

Coverage of the Antarctic by Magsat is limited to latitudes equatorward of 83°. The resulting polar «hole» has a radius of some 700 km. Because the perigee or low point of Magsat's orbit was some 350 km, the effective «hole» (that region in which significant anomalies will be undetected) has a radius of at least 350 km.

The POGO missions cover more of the polar «hole». OGO-2, which flew from 1965 until 1967, collected data at latitudes up to 87°. Its polar «hole» has a radius of some 300 km. The perigee of the OGO-2 orbit was 410 km. This means that there will be no effective «hole» in the OGO-2 anomaly coverage although anomalies within the «hole» will have lower spatial and amplitude resolution. OGO-4 (1967-1969) also collected data at higher latitudes than Magsat. With an inclination of 86° and a perigee of 410 km, there will again be no effective «hole» in the OGO-4 anomaly coverage. Only OGO-6 (1969-1971), with an inclination of 82°, collected data at lower latitudes than Magsat.

The POGO missions cover all local times. Local time coverage is important because the ionospheric dynamo varies as a function of local time. Proper parameterization and removal of the S_q magnetic field originating from the ionospheric dynamo improves our ability to isolate the crustal field contribution.

The POGO missions also cover all seasons. They provide coverage of the Antarctic during the austral winter when the ionospheric dynamo should be least active. This is in contrast to Magsat, which flew only during an austral summer when the polar regions were always in daylight.

2. Previous POGO and Magsat maps

In this section we will review the four state-of-the-art maps of the Antarctic lithospheric magnetic field (fig. 2a-d), discuss some of the salient details of their production, review their limitations, and point out the differences in the maps. For a review of all of the Antarctic anomaly maps made using satellite data, including those of historical interest only, the reader is directed to Langel and Hinze (1998). These authors also have more details concerning the correlation coefficients among the various maps. None of these maps parameterize the external fields in a physically reasonable way. Attempts are underway (Langel *et al.*, 1996) to include the ionosphere, magnetosphere, and their coupling currents along with fields of internal origin in a comprehensive model of the terrestrial magnetic field.

2.1. *POGO*

Langel (1990) used a sequential approach to a global selection of POGO data in attempting to isolate the lithospheric contribution. After removal of a main field model that accounts for the effects of secular variation, the data was selected for: 1) altitude (< 600 km); 2) global planetary magnetic index, $K_p \leq 2_+$; 3) local time less than 09:00 or greater than 15:00, and 4) residual < 20 nT. Subsequent to this selection, adjacent passes were visually intercompared in order to discard passes that contained significant non-correlative parts. Subsets of the remaining passes were then fit with linear functions in order to remove features with wavelengths in excess of 4000 km. These long-wavelength features originate in the ionosphere and

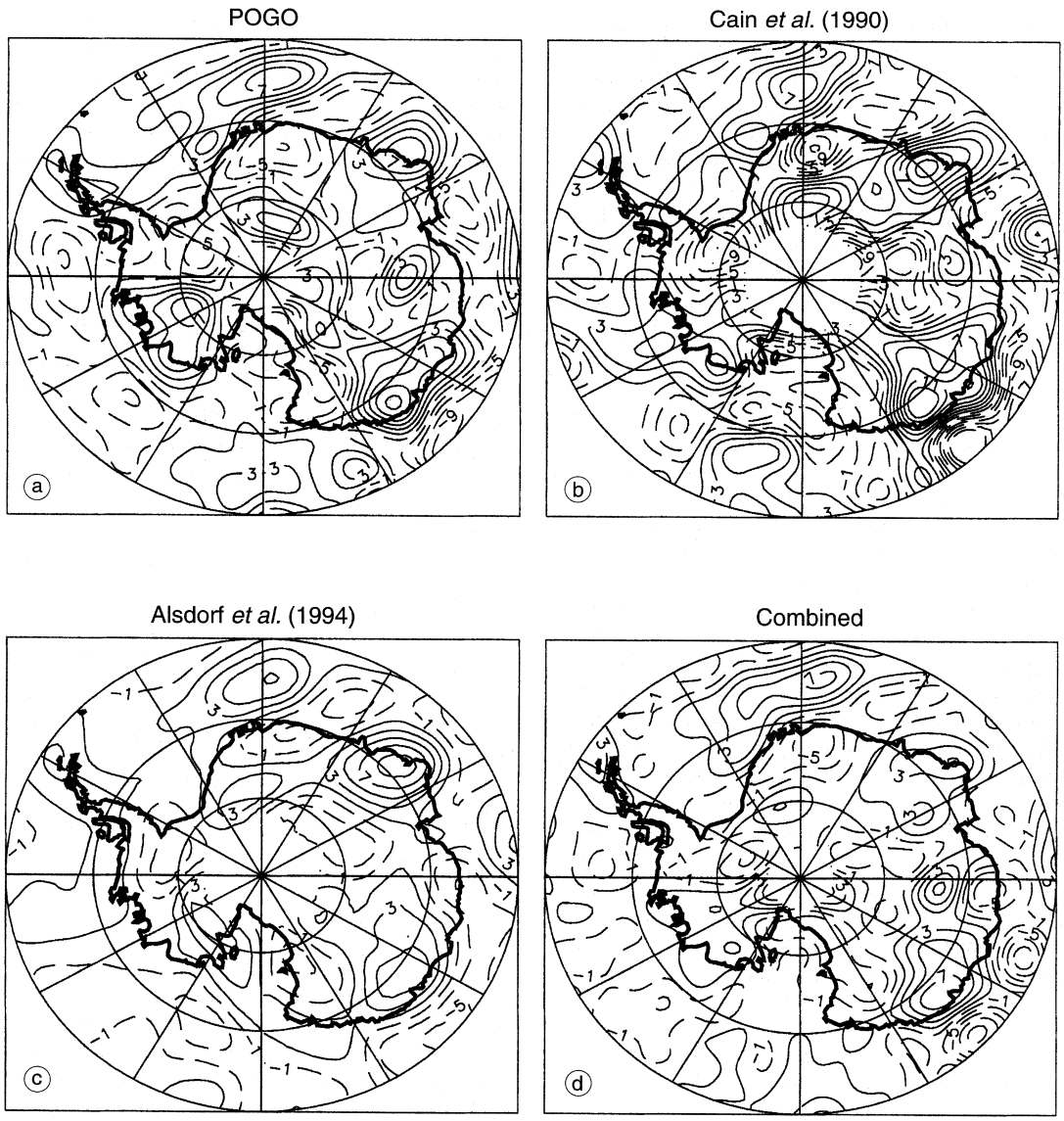

Fig. 2a-d. Previous scalar satellite magnetic anomaly maps using Magsat and/or POGO data. a) Using POGO data of Langel (1990) and Arkani-Hamed *et al.* (1994) in spherical harmonic degree 15-60; b) using Magsat data from spherical harmonic solution (degrees 15-49 only) of Cain *et al.* (1990), termed model M102389; c) using Magsat data from Alsdorf *et al.* (1994) and d) using combined POGO and Magsat data from Arkani-Hamed *et al.* (1994) degrees 15-60. All figures use a stereographic projection and have a contour interval of 2 nT. All maps are at 400 km except for fig. 2c which is at 430 km.

magnetosphere but also contain significant lithospheric components. After removal of these trends, data from the interior of each pass segment were altitude normalized using an equivalent source technique. Subsequent to the publication of these results in Langel (1990), it was realized that spherical harmonic degrees 13 and 14 were contaminated by non-lithospheric fields. These degrees were removed and the scalar field at 400 km calculated from the equivalent source solution is shown in fig. 2a. For further details, the reader is referred to Langel (1990) and Arkani-Hamed *et al.* (1994).

2.2. *Magsat: spherical harmonic model*

Cain *et al.* (1990) used least-squares fitting of a spherical harmonic model to a global selection of Magsat data. The spherical harmonic solution extended to degree 49 and that portion dominated by lithospheric fields, degrees 15-49, is shown in fig. 2b. The model, termed M102389, is discussed further in Cain *et al.* (1990). The data that went into making this model was selected for: 1) $K_p \leq 2_+$, and 2) residual to the M07AV6 model (Cain *et al.*, 1989) of less than 50 nT. Prior to incorporation in the model, a magnetospheric field proportional to an independently derived D_{st} index was removed. This has the effect of retaining some long-wavelength, along-track components. Ionospheric fields were also removed prior to incorporation in the model using the technique of Yanagisawa and Kono (1985) as modified by Cain *et al.* (1989).

2.3. *Magsat: 1 and 2D correlation*

Alsdorf *et al.* (1994) used a multistep approach to a Magsat data set restricted to high southern latitudes in attempting to extract the lithospheric signal. In contrast to the other techniques, Alsdorf *et al.* (1994) select passes based on their variance properties rather than on planetary magnetic indices such as K_p. They also adopt a more quantitative approach than Langel (1990) to the comparison of adjacent passes in order to isolate correlative signals. Each pass is converted into the frequency domain and compared there with the two adjacent passes. Frequency components that are present in all three passes at some spectral correlation level are retained. The data set is divided into four altitude ranges and into dawn and dusk local times. The resultant maps are again converted into the frequency domain and the dawn and dusk maps are compared. Again, correlative frequency components are retained. The maps are then altitude normalized and again compared in the frequency domain. The common features of the four maps are averaged together to produce the final map (fig. 2c). The Alsdorf *et al.* (1994) map differs from the other maps in its use of a non-standard main field model. Instead of removing a single main field model from all passes, a main field model is calculated in a least-squares fashion from each pass.

2.4. *Combined Magsat and POGO*

Arkani-Hamed *et al.* (1994) used the POGO map shown in fig. 2a along with independently derived maps made from the Magsat dawn and dusk local times (Ravat *et al.*, 1995) and combined them in the spherical harmonic domain, retaining only those features that are common to all three maps at some level of correlation. Those common features are shown in fig. 2d. For further details, the reader is referred to Arkani-Hamed *et al.* (1994) and Langel (1995).

3. Robust features of previous maps

Using the POGO map (fig. 2a) as a base, we have qualitatively identified those features which can be seen on all four of the previous maps. Those common features are assigned letters and are shown on fig. 3. While there is general agreement about the relative magnitude of the common features, their absolute magnitude is seen to vary systematically from map to map, with the map of Cain *et al.* (1990) having the highest amplitudes and the map of Alsdorf *et al.* (1994) having the lowest amplitudes. Because the map of Alsdorf *et al.* (1994) was computed at an altitude of 430 km, we expect that its amplitude

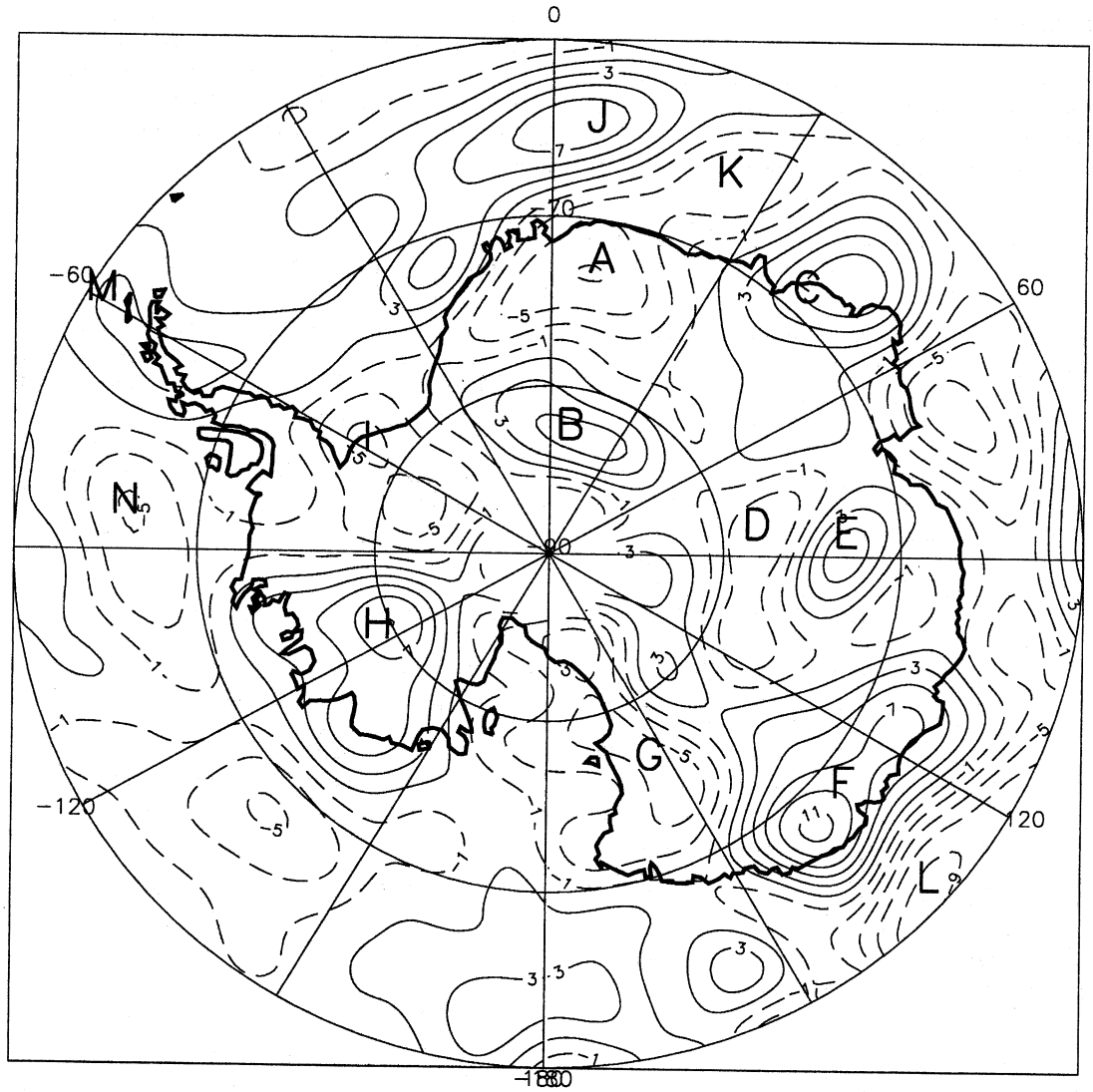

Fig. 3. POGO anomaly map with robust features lettered. Stereographic projection. Contours are in nT. 400 km altitude.

will be reduced relative to the other three maps, computed at 400 km. The higher absolute magnitude of the map of Cain *et al.* (1990) is a global feature (Ravat *et al.*, 1995). It is commonly the case that each additional processing step will remove some of the signal in addition to removing more of the noise. If this is the case, then the higher absolute magnitude of the map of Cain *et al.* (1990) could be a consequence of their smaller number of processing steps. It may also be that the deliberate attempt by Cain *et al.* (1990) to minimize along-track filtering or its equivalent has resulted in a map with higher amplitudes.

4. Modeling

In an attempt to explain some of the persistent anomalies detailed in the previous section, we have constructed a forward model of the Antarctic continental and oceanic lithosphere. This forward model has two components: 1) the 3SMAC model of Nataf and Ricard (1996), based on seismic and heat flow observations, and 2) the distribution of Cretaceous Quiet Zone oceanic crust from marine geomagnetic surveys.

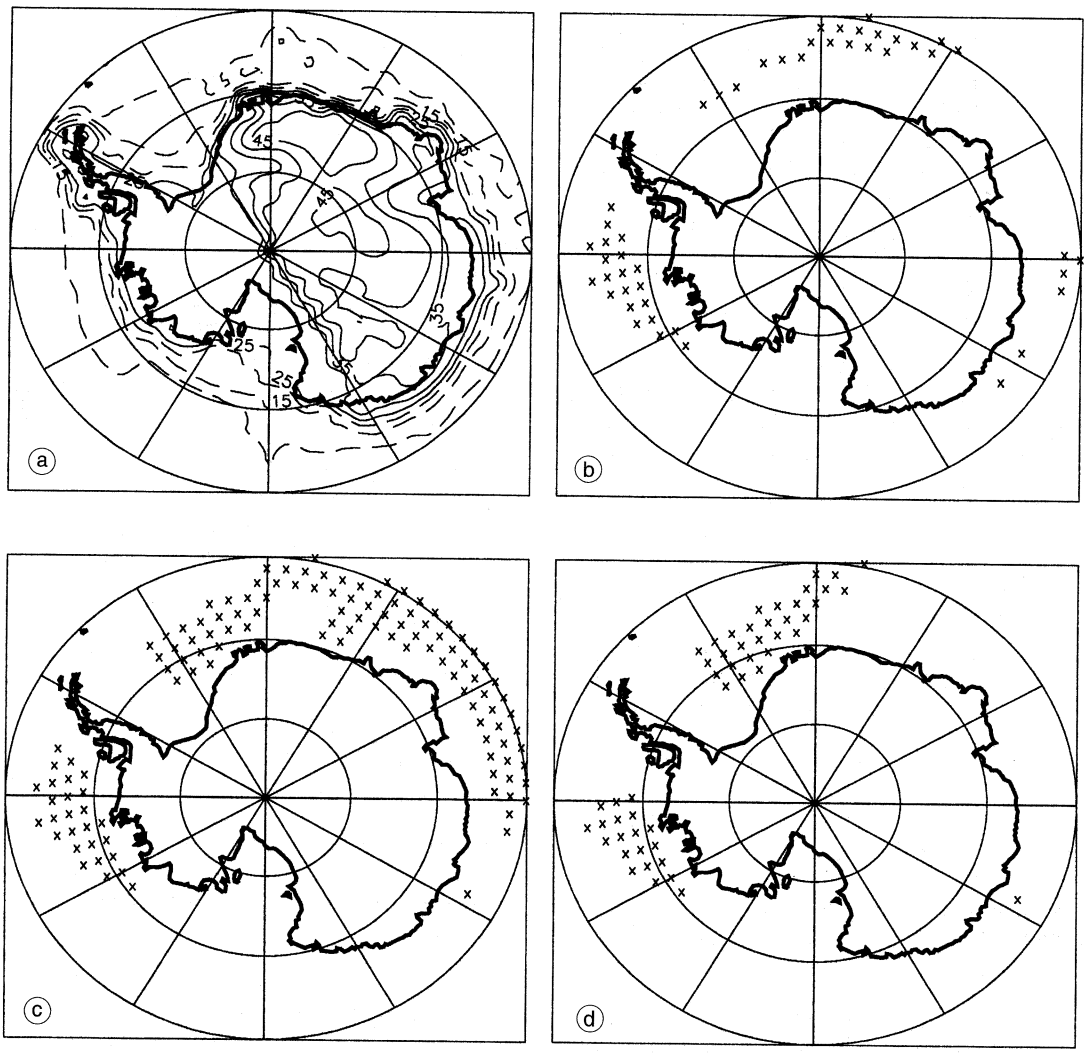

Fig. 4a-d. Model parameters. a) Magnetic crustal thickness (km) from 3SMAC model (Nataf and Ricard, 1996). Contour interval is 5 km. Contours less than 25 km are shown as dashed lines; all others are shown as solid lines. b) Cretaceous Quiet Zone crust from Müller *et al.* (1997) shown as *x*'s. The *x*'s locate the position of magnetic dipoles used in the modeling. Dipole spacing is 1.89°. c) Cretaceous Quiet Zone crust from Sclater *et al.* (1981). d) Best-fit Cretaceous Quiet Zone crust. All figures use a stereographic projection.

The 3SMAC model contains estimates of the thickness of the igneous and sedimentary crust on a 2° grid worldwide and also a tectonic regionalization from which to predict heat flow and hence an estimate of the Curie point isotherm. In order to calculate the thickness of the magnetic crust (fig. 4a) from the 3SMAC model, the igneous crustal thickness is reduced by that portion which has a temperature greater than the Curie point of magnetite, taken to be 570 °C. The susceptibility chosen for the continental crust was 0.035 SI; for the oceanic crust the chosen susceptibility was 0.04 SI. For further details concerning the use of this model in magnetics, the reader is directed to Purucker *et al.* (1998). This simple model only accounts for susceptibility or remanent magnetizations in the direction of the inducing field. Inadequacies of the model in the Antarctic include little detail of the Bentley subglacial trench and the surrounding West Antarctic rift system.

In the oceanic realm, fields from the alternating normal and reverse remanent magnetizations of the oceanic seafloor are nearly cancelled at satellite altitude. However, coherently magnetized oceanic crust associated with the Cretaceous Quiet Zone (KQZ) is extensive enough to result in measurable magnetic fields at satellite altitude (LaBrecque and Raymond, 1985). Because the distribution of Cretaceous Quiet Zone crust around the Antarctic is poorly known, we have used 3 different models in our simulations. The first model (fig. 4b) is due to Müller *et al.* (1997) and includes only those KQZ areas for which there is compelling evidence. The second model (fig. 4c) is a more permissive model (Sclater *et al.*, 1981) that relies on extrapolation from the more well known KQZ areas. The third model (fig. 4d) is the authors' attempt to incorporate elements from both Müller *et al.* (1997) and Sclater *et al.* (1981) in a forward model that fits more of the robust observations (fig. 3). The KQZ crust is assigned a magnetization of 3.9 A/m, equivalent to a susceptibility of 0.1 SI in an ambient field of 50000 nT. The magnetization is assumed to lie in the direction of the inducing field.

The forward modeling technique is detailed in Purucker *et al.* (1998) and is done globally using equivalent source dipoles (Dyment and Arkani-Hamed, 1998a; Von Frese, 1998). The mathematical development of the equivalent source dipole technique used by the GSFC group in this paper is based on work published in the «grey» literature by Mayhew *et al.* (1984) and it is identical with the work of Dyment and Arkani-Hamed (1998a). Subsequent to the calculation of the field, components that overlap with the core field (degrees 1-13) are removed. The results are shown in fig. 5a-d.

5. Interpretation

Our interpretation will focus on those modeled anomalies on fig. 5a-d which are seen on all of the observed maps (fig. 3, in capital letters). Those modeled anomalies which are present on the map of observations are located with a number on fig. 5a,d and are tabulated in table I in order of decreasing confidence.

The Wilkes Land positive anomaly, shown as F on fig. 3, corresponds to modeled anomaly 1 (fig. 5d). The observed anomaly has its origin in its location on a «corner», in the contrasting thickness of continental and adjacent oceanic crust, in the magnetic thickness contrast between the East and West Antarctic cratons shown in fig. 4a, and in lateral variations in magnetic properties (Von Frese *et al.*, 1986) established prior to the breakup of Pangea.

The Antarctic peninsula positive anomaly, shown as M on fig. 3, corresponds to modeled anomaly 2 (fig. 5d). The cause of the anomaly is related to the contrasting thickness of the island arc and adjacent oceanic crust.

The elongate positive anomaly (J, fig. 3), centred over but more extensive than the Maud Rise, corresponds to modeled anomaly 3 (fig. 5d). The anomalies presence in the model is related to the presence of KQZ crust in the area. Based on our modeling, there is probably more KQZ crust than indicated by Müller *et al.* (1997). The KQZ distribution may be closer to the map of Sclater *et al.* (1981). The contribution of the Maud Rise, an oceanic plateau, to the observed anomaly, is unknown but may be significant (Fullerton *et al.*, 1994). Serpentinization may also play a role.

The positive anomaly (C, fig. 3) over Enderby Land and the Cosmonaut Sea probably cor-

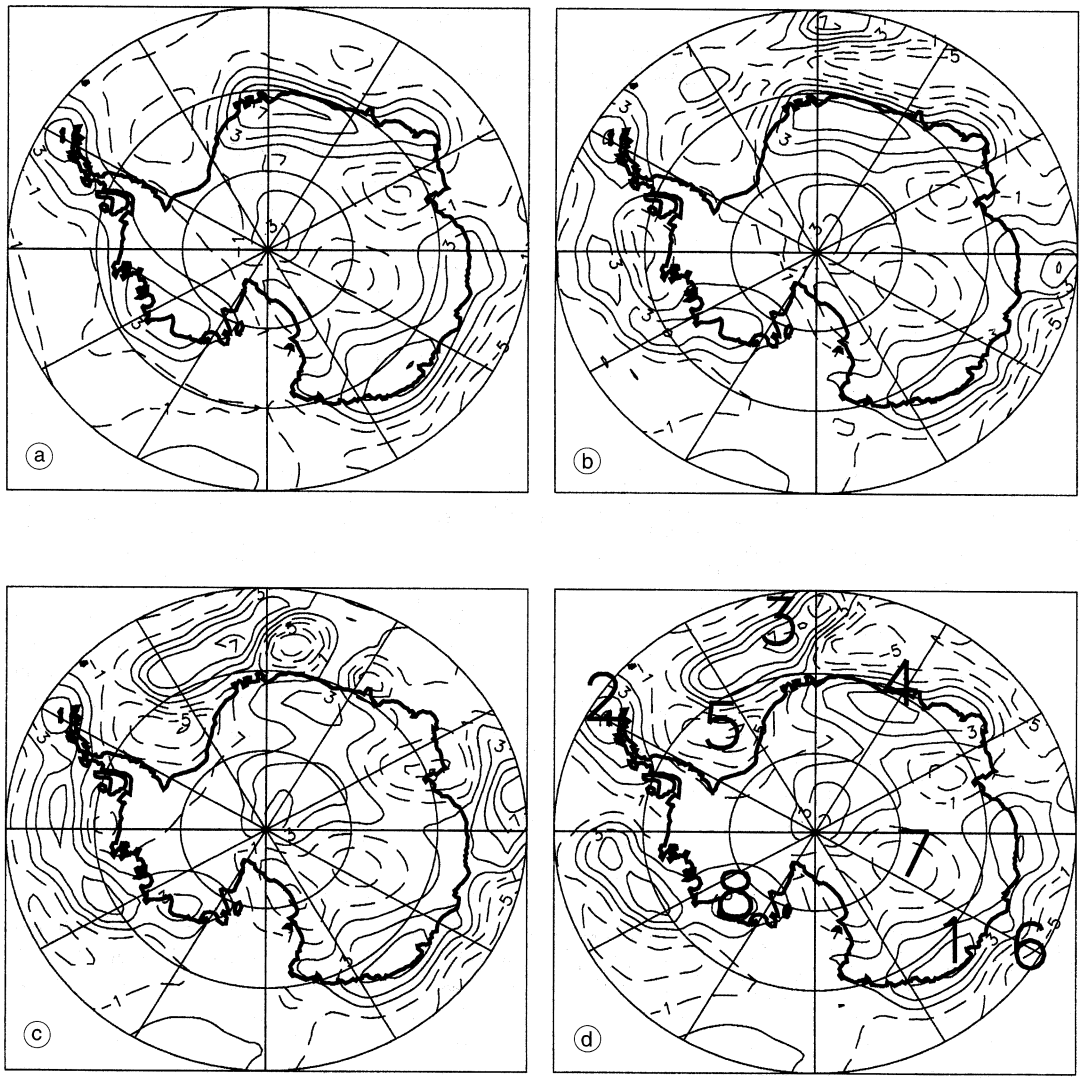

Fig. 5a-d. Scalar field calculated from model parameters shown in fig. 4a-d. a) Using only magnetic crustal thickness contrast from fig. 4a. Continents assigned magnetic susceptibility of 0.035 SI, oceans are assigned 0.04 SI. b) Using magnetic crustal thickness contrast and contrast provided by Müller *et al.* (1997) distribution of Cretaceous Quiet Zone (KQZ) crust shown in fig. 4b. KQZ crust is assigned a susceptibility equivalent to 0.1 SI in a 50 000 nT field. c) Using magnetic crustal thickness contrast and contrast provided by Sclater *et al.* (1981) distribution of KQZ crust shown in fig. 4c. d) Using magnetic crustal thickness contrast and contrast provided by a best-fit distribution of KQZ crust shown in fig. 4d. All figures use a 2 nT contour interval and a stereographic projection. Large numbers on fig. 5d correspond to robust observed anomalies. 400 km altitude.

Table I. Correspondence of robust observations with model anomalies. Compiled in order of decreasing confidence.

Observation (fig. 3)	Model (fig. 5d)	Explanation
F	1	Multiple
L	6	Contrasting thickness (continent/ocean)
M	2	Contrasting thickness (arc/ocean)
J	3	Cretaceous Quiet Zone
C	4	Multiple
I	5	Contrasting thickness ??
D	7	Contrasting thickness ??
H	8	Contrasting thickness

responds to modeled anomaly 4 (fig. 5d). The anomaly's presence in the model is related to the contrasting thickness of the Enderby Land continental crust and adjacent oceanic crust, as modified by the distribution of KQZ crust. The observed anomaly may also be related to lateral variations of magnetization in the iron-rich Archean and Proterozoic rocks of Enderby Land (Harley, 1991). Based on our modeling, the areal extent of KQZ crust is probably closer to the digital map of Müller *et al.* (1997). The observed positive anomaly does not extend over Dronning Maud Land, as it does in the models, suggesting that the magnetic crust may be thinner, or with less contrast, than shown on fig. 4a.

The negative anomaly (I, fig. 3) over the Ellsworth Mountains and including the Dufek Massif, may correspond to modeled anomaly 5. The cause of the anomaly is related to the contrasting thickness of the continental and oceanic crust there. The anomalies greater landward extend in the observations may suggest a thinner magnetic crust under the Ellsworth Mountains and adjacent parts of Marie Byrd Land.

The positive anomaly (H, fig. 3) over most of Marie Byrd Land may correspond to modeled anomaly 8. The anomaly's presence in the model is related to the contrasting thickness of the continental and oceanic crust there. There is no evidence in the magnetic observations for the presence of KQZ crust offshore, in contrast to their presence in the models of Müller *et al.* (1997) and Sclater *et al.* (1981). The anomaly's coincidence with a rift, the Bentley subglacial trench, may also play a role in the location and magnitude of the observed anomaly.

Finally, we should point out those features (A, B, E, G, N, and K, fig. 3) which show little or no correspondence with anomalies in our simple models. These anomalies may be related to lateral variations of magnetization, inadequate models of the magnetic crustal thickness, or perhaps to remanent magnetizations in directions other than the present field.

6. Future directions

The complete POGO data set has only recently become available in digital form from the National Space Science Data Center and hence it is appropriate to consider how it might be used to improve anomaly maps of the Antarctic region. As discussed in the introduction, Magsat flew only during the austral summer when the south polar region was in constant light. Some of the reproducibility problems encountered in producing crustal magnetic anomaly maps here may be attributed to the greater activity of the ionospheric dynamo during daylight hours.

The availability of a large (> 5 Gb of data with a sample collected every 0.5 s) magnetic field data set means that the data set can be subdivided by multiple criteria in order to search for the static signal and to eliminate excessively contaminated observations. For example, in addition to a subdivision into austral summer and

winter, the POGO data can also be subdivided by external field indices such as the $F_{10.7}$ solar flux, D_{st}, and the IMF, reflecting the ionosphere, magnetosphere, and solar wind influences, respectively. The POGO data set can also be finely subdivided by local times, continuing the work of Langel (1990) in his study of the POGO anomaly field. Previous studies of the anomaly field as measured by the POGO satellites have relied on visual comparison of adjacent passes and the removal of linear functions from subsets of individual passes.

The POGO satellites also cover more of the polar hole, as mentioned in the introduction. This will allow a detailed examination of anomalies poleward of 83°S latitude. As can be seen from fig. 6, there is adequate coverage for mapmaking in this region, even restricting the data

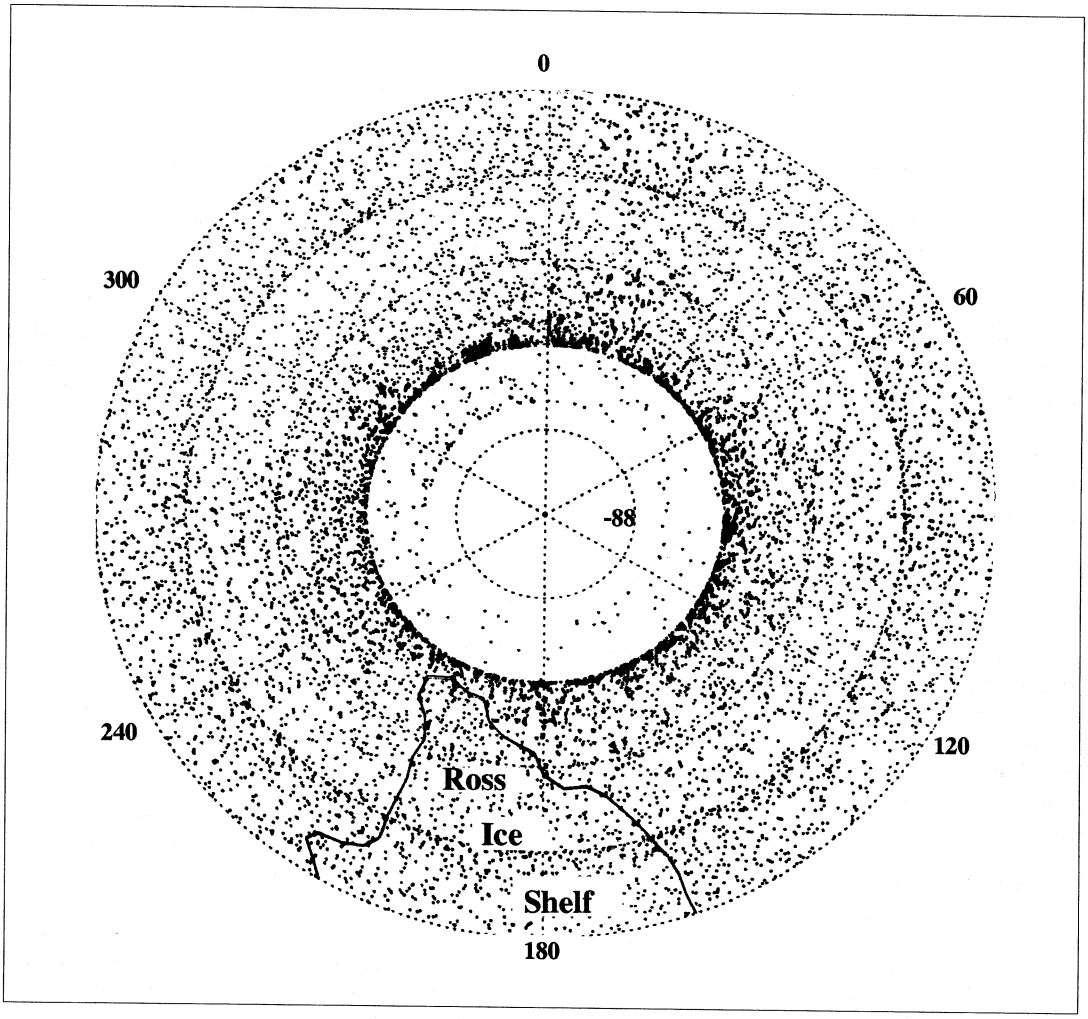

Fig. 6. Distribution of POGO data in austral winter from 80°S to the south pole. Plot shows the location of all data with altitudes less than 500 km. Altitudes on the POGO CD-ROMs available from the National Space Science Data Center are geocentric altitudes relative to a spherical earth of radius 6371.0 km.

set to the low altitude band where the anomalies should be largest, and the austral winter when the ionosphere is least disturbed. As can be seen from fig. 3, the POGO data shows several substantial anomalies in the polar hole. These will need to be validated by comparison of maps made at different seasons and local times.

The improvement of the remanence model used in the prediction of magnetic anomalies in the oceanic realm should be possible using the recent work of Dyment and Arkani-Hamed (1998b), who incorporate information on remanent direction and shorter polarity zones in their model. Improvements will also come from an Indian Ocean geophysical compilation project now underway (J.G. Sclater, personal communication) and from new information in the Weddell Sea (Livermore and Hunter, 1996).

The goal of our work is to produce a robust map of the lithospheric anomaly field as seen from satellite. This should be useful in the compilation of ADMAP. The satellite map can be downward continued to aeromagnetic survey altitude and used to level the aeromagnetic surveys. We hope to be able to provide the missing longest wavelength anomaly components which are not recovered during the amalgamation of disparate aeromagnetic surveys (Arkani-Hamed and Hinze, 1990).

Acknowledgements

We thank D. Ravat for a review of an early version of the manuscript. Suggestions made by the referees (D. Alsdorf and A. De Santis) substantially improved the manuscript. Supported by NASA RTOP 579-31-01, for which we are grateful.

REFERENCES

ALSDORF, D.E., R.R.B. VON FRESE, J. ARKANI-HAMED, and H.C. NOLTIMIER (1994): Separation of lithospheric, external, and core components of the south polar geomagnetic field at satellite altitudes, *J. Geophys. Res.*, **99**, 4655-4668.

ARKANI-HAMED, J.R. and W.J. HINZE (1990): Limitations of the long-wavelength components of the North American magnetic anomaly map, *Geophysics*, **55**, 1577-1588.

ARKANI-HAMED, J., R. LANGEL and M. PURUCKER (1994): Scalar magnetic anomaly maps of Earth derived from POGO and Magsat data, *J. Geophys. Res.*, **99**, 24075-24090.

CAIN, J.C., R.A. LANGEL and S.J. HENDRICKS (1967): First magnetic field results from the OGO-2 satellite, *Space Res.*, **7**, 1467.

CAIN, J.C., Z. WANG, C. KNUTH and D.R. SCHMITZ (1989): Derivation of a geomagnetic model to $n = 63$, *Geophys. J.*, **97**, 431-441.

CAIN, J.C., B. HOLTER and D. SANDEE (1990): Numerical experiments in geomagnetic modeling, *J. Geomagn. Geoelectr.*, **42**, 973-987.

DYMENT, J. and J. ARKANI-HAMED (1998a): Equivalent source magnetic dipoles revisited, *Geophys. Res. Lett.*, **25**, 2003-2006.

DYMENT, J. and J. ARKANI-HAMED (1998b): Contribution of lithospheric remanent magnetization to satellite magnetic anomalies over the world's oceans, *J. Geophys. Res.*, **103**, 15423-15441.

FULLERTON, L.G., H.V. FREY, J.H. ROARK and H.H. THOMAS (1994): Contributions of Cretaceous Quiet Zone natural remanent magnetization to Magsat anomalies in the Southwest Indian Ocean, *J. Geophys. Res.*, **99**, 11923-11936.

HARLEY, S.L. (1991): The crustal evolution of some East Antarctic granulites, in *Geological Evolution of Antarctica*, edited by M.R.A. THOMSON *et al.* (Cambridge University Press, Cambridge), 7-12.

LABRECQUE, J.L. and C.A. RAYMOND (1985): Seafloor spreading anomalies in the Magsat field of the North Atlantic, *J. Geophys. Res.*, **90**, 2565-2575.

LANGEL, R.A. (1982): The magnetic earth as seen from Magsat, initial results, *Geophys. Res. Lett.*, **9**, 239-242.

LANGEL, R.A. (1990): Global magnetic anomaly maps derived from POGO spacecraft data, *Phys. Earth Planet. Inter.*, **62**, 208-230.

LANGEL, R.A. (1995): An investigation of a correlation/covariance method of signal extraction, *J. Geophys. Res.*, **100**, 20137-20157.

LANGEL, R.A. and W.J. HINZE (1998): *The Magnetic Field of the Earth's Lithosphere: the Satellite Perspective* (Cambridge University Press), pp. 325.

LANGEL, R.A., T.J. SABAKA, R.T. BALDWIN and J.A. CONRAD (1996): The near-Earth magnetic field from magnetospheric and quiet-day ionospheric sources and how it is modeled, *Phys. Earth Planet. Inter.*, **98**, 235-267.

LIVERMORE, R.A. and R.J. HUNTER (1996): Mesozoic seafloor spreading in the Southern Weddell Sea, in *Weddell Sea Tectonics and Gondwana Break-up*, edited by B.C. STOREY *et al.*, *Geol. Soc., London, Spec. Publ.*, **108**, 227-241.

MAYHEW, M.A., R.H. ESTES and D.M. MYERS (1984): Remanent magnetization and three-dimensional density model of the Kentucky anomaly region, *Business and Technological System Report BTS07-84-121* to NASA, pp. 25.

MÜLLER, R.D., W.R. ROEST, J.Y. ROYER, L.M. GAHAGEN and J.G. SCLATER (1997): Digital isochrons of the ocean floor, *J. Geophys. Res.*, **102**, 3211-3214.

NATAF, H. and Y. RICARD (1996): 3SMAC: An *a priori* tomographic model of the upper mantle based on geophysical modeling, *Phys. Earth Planet. Inter.*, **95**, 101-122.

OLSEN, N. (1999): Induction studies with satellite data, *Surv. Geophys.* (in press).

PURUCKER, M.E., R.A. LANGEL, M. RAJARAM and C. RAYMOND (1998): Global magnetization models with *a priori* information, *J. Geophys. Res.*, **103**, 2563-2584.

RAVAT, D., R.A. LANGEL, M. PURUCKER, J. ARKANI-HAMED and D.E. ALSDORF (1995): Global vector and scalar Magsat magnetic anomaly maps, *J. Geophys. Res.*, **100**, 20111-20136.

REGAN, R.D., J.C. CAIN and W.M. DAVIS (1975): A global magnetic anomaly map, *J. Geophys. Res.*, **80**, 794-802.

SCLATER, J.G., B. PARSONS and C. JAUPART (1981): Oceans and continents: similarities and differences in the mechanisms of heat loss, *J. Geophys. Res.*, **86**, 11535-11552.

TARITS, P., N. GRAMMATIKA and J. DYMENT (1997): Modelling of long wavelength magnetic anomalies in terms of electrical conductivity heterogeneities (abstract), in *IAGA 8th Scientific Assembly, Uppsala, Sweden*, p. 487.

VON FRESE, R.R.B. (1998): Correction to R.R.B. von Frese, W.J. Hinze and L.W. Braille, Spherical Earth Gravity and Magnetic Anomaly Analysis by Equivalent Point Source Inversion, *Earth Planet. Sci. Lett.*, **163**, 409-411.

VON FRESE, R.R.B., W.J. HINZE, R. OLIVIER and C.R. BENTLEY (1986): Regional magnetic anomaly constraints on continental breakup, *Geology*, **14**, 68-71.

YANAGISAWA, M. and M. KONO (1985): Mean ionospheric field corrections for Magsat data, *J. Geophys. Res.*, **90**, 2527-2536.